ACS APPLIED MATERIALS & INTERFACES

Forum Article

www.acsami.org

Aptamer-Functionalized Gold Nanoparticles As Photoresponsive Nanoplatform for Co-Drug Delivery

Yi-Syun Shiao, Huai-Hsuan Chiu, Pin-Hsuan Wu, and Yu-Fen Huang*

Department of Biomedical Engineering and Environmental Sciences, National Tsing Hua University, Hsinchu, Taiwan ROC

Supporting Information

ABSTRACT: Various platforms have been developed as innovative nanocarriers to deliver therapeutic agents to the diseased sites. Multifunctional surface modification allows an enhanced recognition and uptake of drug carriers by targeted cells. However, the development of drug resistance in some tumor cells plays a major role in the failure of chemotherapy. Drugs given in combination, called multidrug delivery approach, was designed to improve the therapeutic efficacy and has become an increasingly used strategy that is of great importance in clinical cancer treatments. In this study, aptamer-functionalized gold nanoparticles (Au NPs) have been used as a nanoplatform to codeliver two different anticancer drugs for improving the drug effectiveness. The surface of Au NPs (13 nm in diameter) was assembled with AS1411 aptamers, which tethered with 21-base pairs of $(CGATCGA)_3$ sequence approached to the Au NPs. Both the photosensitizer 5,10,15,20-tetrakis(1-methylpyridinium-4-yl) porphyrin ($TMPyP_4$) and the chemotherapeutic drug doxorubicin (Dox) were then physically attached to the AS1411-conjugated Au NPs (T/D:ds-NPs) and delivered to the target tumor cells such as HeLa and Dox-resistant MCF-7R cell lines. When exposed to a 632 nm light, reactive oxygen species induced by $TMPyP_4$ molecules were generated inside the living cells, followed by cell damage. In addition, triggered release of the complementary drugs also occurred simultaneously during the photodynamic reaction. In the presence of Dox molecules, the toxicity toward the target cells was superior to individual drug treatment. Overall, a co-drug delivery platform was successfully established to improve the therapeutic efficacy in tumor cells. The improvement of the photodynamic-stimulated triggered release was enhanced, thus highly promising precise drug release in targeted drug delivery.

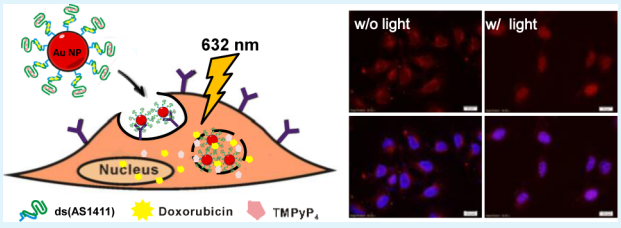

KEYWORDS: *aptamer, gold nanoparticle, photodynamic therapy, chemotherapy, multidrug resistant*

INTRODUCTION

Photodynamic therapy (PDT) has emerged as a popular, noninvasive treatment for numerous cancers such as inoperable esophageal tumors and malignancies of the head and neck.[1−3] It also gained worldwide popularity in adjunctive treatments for other cancer types, including breast, prostate, and ovarian in preclinical and clinical trials.[4−6] The basic principle of PDT involves the administration of photosensitizing agents followed by local illumination of the target tissue with a light source. A sufficient amount of molecular oxygen (normally present in the tumor) is also required to achieve effective treatment. The collision of an oxygen molecule with the photoexcited sensitizer results in the formation of $^1O_2$ and other reactive oxygen species (ROS) that cause oxidative damage to cellular components. It may also destroy the tumor vasculature, thereby depriving the tumor of oxygen and nutrients and ultimately, leading to tumor cell death.

Most photosensitizers used in PDT are water-insoluble.[7,8] They exhibit high level of dark toxicity, rapid degradability, and consequent inactivity under irradiation, therefore restricting their clinical applications. To address these issues, numerous drug formulations have been extensively studied as potential PDT agents. The use of nanoparticles as delivery vehicles is likely one of the most promising strategy in cancer research.[9−13] A wide range of biocompatible, nontoxic nanoparticles such as liposomes and polymer-, silica-, magnetic-, gold-, and carbon-based NPs have been developed to improve the efficacy of PDT.[14−29] Nanoparticles localize to the tumor via the enhanced permeability and retention (EPR) effect or active targeting over free drugs. The achievement of high drug accumulation into a tumor allows effective reduction of side effects associated with PDT treatment. Furthermore, nanoparticles can protect photosensitizers from leakage, degradation, or modification in the biological environment prior to delivery of the drug to the infected tissues.

With the recent interests in multimodality, nanoparticles that can incorporate different functionalities are attractive candidates for advanced medical applications. For example, PDT based on upconversion nanoparticles (UCNPs)[30−33] has been developed as a new approach to deliver near-infrared light into deeper tissues for PDT treatment. UCNPs, which offer unique upconversion luminescence, are beneficial for remarkably

Special Issue: Materials for Theranostics

Received: April 29, 2014
Accepted: June 11, 2014
Published: June 20, 2014

sensitive in vivo biomedical imaging and cell tracking. Several other image-guided involvements of PDT deliveries, e.g., magnetic resonance (MR) imaging have also been presented by different groups in recent years.[22,34−36] The combination of both therapeutic and diagnostic capabilities in one dose makes these nanoparticles ideal platforms for theranostics. In addition, the simultaneous delivery of anticancer drugs and photosensitizers to the tumor cells is expected to overcome the hurdles of traditional single-drug treatments.[37−40] Nanoparticle-mediated combination of chemotherapy and PDT has been investigated to overcome drug resistance in mouse tumor model by invoking multiple anticancer mechanisms.[41] A significant enhancement of ROS production and cytotoxicity using nanoparticles contributes to the greatly improved efficacy of combination treatment.

Despite the above-mentioned advantages, photodynamic reaction is less commonly used in remote-controlled release other than the potential triggers such as light, ultrasound, and magnetic field. Only a few successful models including cyclodextrin dimers and pro-drug molecules have been designed to be photocleavable in response to the singlet oxygen generation.[42−44] On the basis of these fundamental concepts, we report a novel nanoscale delivery platform, in which photoinduced ROS generation is employed to trigger drug release. As depicted in Scheme 1, nucleolin-specific, aptamer-conjugated gold nanoparticles were constructed to serve as effective carriers for both anticancer drugs, doxorubicin (Dox), and photosensitizer ($TMPyP_4$). When exposed to optimal light, photoactivated sensitizers generate a burst of ROS. The rapid reaction with the nearby DNA hosts subsequently leads to liberation of therapeutic effective agents in a specific manner. To the best of our knowledge, this is the first study presenting an engineered nanoparticle for co-drug delivery in response to the PDT process. Eventually, the combination of PDT and chemo-cytotoxicity yields a synergistic therapeutic effect that overcomes tumor drug resistance.

Scheme 1. Schematic Illustration of the Co-Drug-Loaded Aptamer-Functionalized Delivery Platform on the Basis of Gold Nanoparticles [a]

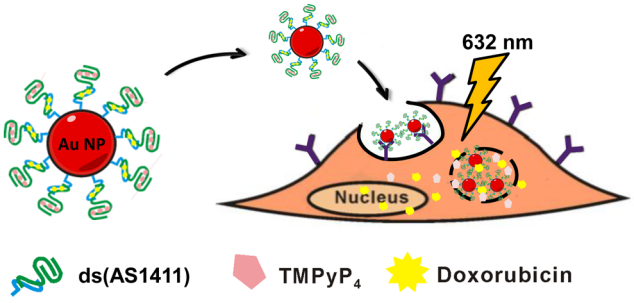

AS1411 aptemr-T_6-$(CGATCGA)_3$: 5'-(GGTGGTGGTGGTTGTGGTGGTGGTGG)-TTTTTT-(CGATCGA CGATCGA CGATCGA)-3'
Complementary sequence: 5'-ThioMC6-TTTTTTTTTT-(TCGATCG TCGATCG TCGATCG)-3'

[a]Effective therapeutic efficacy overcomes tumor drug resistance, which was accomplished by the established nanoparticle-mediated combination therapy followed by light illumination.

RESULTS AND DISCUSSIONS

To demonstrate the effectiveness of our approach, we used an nucleolin-specific AS1411 aptamer with a 27-base $T_6(CGATCGA)_3$ sequence extension at the 3′ end.[45] After hybridization with the complementary sequence 5′ thiol-$T_{10}(TCGATCG)_3$, multiple copies of double-stranded DNA [ds(AS1411)] were assembled onto the surface of Au NPs via strong gold−thiol linkages (Scheme 1). The 10 extra T bases at the 5′-terminus ensure that the binding domains of the aptamer extend away from the Au NP surface. An increase in the hydrodynamic diameter from 19.9 ± 0.6 nm of citrate-stabilized Au NPs to 38.7 ± 1.4 nm of ds(AS1411)-Au NPs confirmed the successful immobilization of ds(AS1411) onto the surface of Au NPs (Figure 1A). The consecutive CG base pairs designed within the extended region ensure high drug-loading capacity, providing binding sites for at least 4−5 Dox molecules.[46,47] With a serial washing/centrifugation procedure, the amount of Dox loaded onto each NP was indirectly determined by measuring the fluorescence signal of the molecules removed from the Dox-loaded ds(AS1411)-Au NP conjugates (D:ds-NPs). After fitting a nonlinear regression equation, acquired from the Scatchard analysis, at various concentrations of free (unbound) Dox, the quantified saturation number was 280 ± 23 Dox molecules per NP. The maximum loading efficiency of Dox was found to be 81 ± (7)% on the basis of following equation: loading efficiency = [residual amount of drug in the nanoparticles/feeding amount of drug] × 100.

Furthermore, the D:ds-NP solution was titrated with a serial concentration of $TMPyP_4$ and the supernatant after each centrifugation was collected and analyzed by fluorescence spectrophotometry to study the interaction between $TMPyP_4$ and the D:ds-NP conjugates. The fluorescence signals at the emission wavelength of 715 nm were then converted to molar concentrations of the $TMPyP_4$ by interpolation from a predetermined standard linear calibration curve. Almost no release of Dox molecules was observed during the conjugation process. By fitting with the Scatchard equation (see Figure S1A in the Supporting Information), the binding ratio of $TMPyP_4$ to each D:ds-NP was 302 ± 13. The maximum loading efficiency of $TMPyP_4$ was calculated to be 87 ± (4)%. This is consistent with previous results[48] revealing that the approximate binding number of $TMPyP_4$ per AS1411 aptamer was 5, when each NP possessed 74 ± 4 ds(AS1411). The Hill plot displayed in Figure S1B (see the Supporting Information) also exhibited fluorescence quenching of $TMPyP_4$ as a function of increasing D:ds-NP concentration. The dissociation constant (K_d = 1.2 ± 0.1 nM) derived from this result indicated that a stable co-drug ($TMPyP_4$/Dox)-loaded nanoplatform (T/D:ds-NPs) was successfully constructed via physical (noncovalent) conjugation.

The stability of the T/D:ds-NP conjugates in high salinity condition was further studied by UV−vis absorption spectra (Figure 1B). The binding of ds(AS1411) onto the surface of Au NPs greatly increases their stability in physiological environments. Spectrophotometric analysis revealed only a slight change in the NPs' peak absorbance after suspension in saline, confirming the successful retention of Au NP stability using thiolated dsDNA. In addition, the observation of the typical absorption band of $TMPyP_4$ at the wavelength of 435 nm from both $TMPyP_4$-loaded ds-NPs (T:ds-NPs) and T/D:ds-NPs also suggested the strong interaction between $TMPyP_4$ and G-quadruplex DNA aptamers assembled on the nanoparticles.[48] This result is in good agreement with the data obtained from zeta-sizer measurements. After immobilization of ds(AS1411), the dsDNA-conjugated Au NPs showed a more negative ζ-

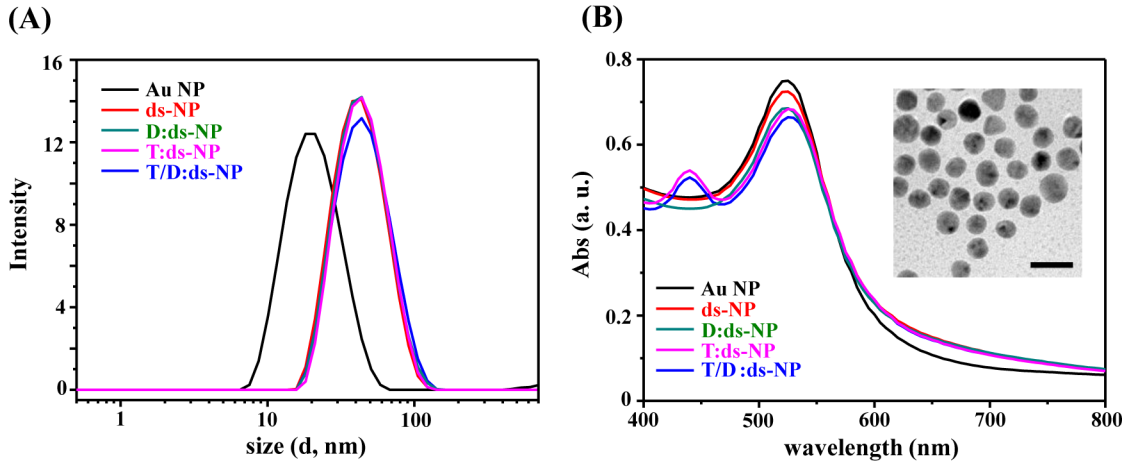

Figure 1. (A) Hydrodynamic size distribution and (B) UV−vis spectra of Au NPs (in 4 mM citrate buffer), ds-NPs, T:ds-NPs, D:ds-NPs, and T/D:ds-NPs (1 ×). Buffer: 10 mM phosphate buffer, 100 mM NaCl, pH 7.4. The concentration of the as-prepared Au NP is denoted as 1×, which corresponds to the concentration of approximately 13 nM. Inset: TEM images of the as-prepared T/D:ds-NPs (scale: 25 nm).

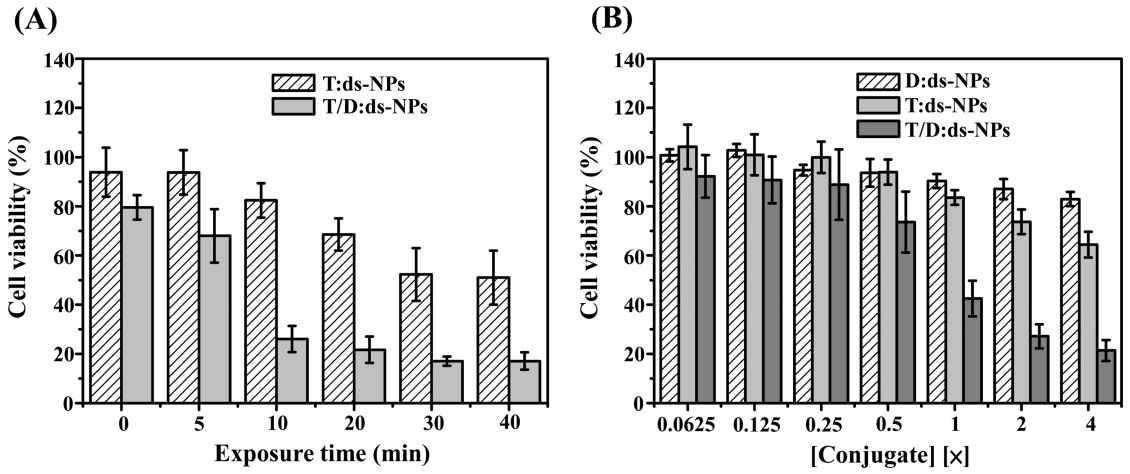

Figure 2. (A) Dependence of cytotoxicity of treated HeLa cells as a function of exposure time (632 nm red light). Cells were incubated with T:ds-NPs and T/D:dsNPs (4×) in washing buffer (1% BSA) at 37 °C for 4 h. After treatments, cells were subsequently grown in fresh culture medium (10% FBS) for 24 h. Cytotoxicity was measured with the MTT assay. (B) Cell viability of HeLa cells under different treatments in washing buffer (1% BSA) at 37 °C for 4 h, followed by red light exposure (632 nm, 20 min).

potential (−44.9 ± 2.8) than the citrate-stabilized Au NPs (−36.0 ± 2.7). Moreover, the subsequent loading of drug molecules (both Dox and $TMPyP_4$) lead to a slight decline in the negative intensity of ζ-potential (−39.4 ± 1.6 mV), whereas the size of the conjugates increased slightly to 40.1 ± 1.4 nm. These results suggested that dsDNA and drug molecules were sequentially introduced onto the surface of Au NPs.

After confirming the physiochemical properties of the drug-loaded ds-NPs, the interaction between the aptamer-functionalized nanocarrier toward cancer cells was investigated using dark-field microscopy coupled to a CCD digital camera. HeLa cells, which overexpress nucleolin on the cell surface,[49] were incubated with T/D:ds-NPs for 4 h, followed by repeated washing steps to remove excess conjugates from the cells. As shown in Figure S2A (see the Supporting Information), the yellow color representing the scattering light from Au NPs was observed in/on the cells, while the untreated control cells appeared dim white because of the intrinsic cellular scattering. To further confirm the intracellular uptake of aptamer-based nanocomplex by HeLa cells, we used trypsin to remove surface-bound particles. The number of ds(AS1411)-NPs taken up by Hela cells was then evaluated via atomic absorption spectrometry (AAS; AAnalyst 600; PerkinElmer, Waltham, MA, USA). Our results showed that the maximum number of ds(AS1411)-NPs inside HeLa cells was 1.5 ± 0.3 × 10^5 per cells, whereas <6.1 ± 0.9 × 10^4 Au NPs were determined for nonspecific intracellular uptake using dsDNA-Au NPs lacking AS1411 [denoted as ds(ctrl)-NPs]. To evaluate the function of ds(AS1411) in the cellular uptake of the aptamer-conjugated complex, a simple competition assay was conducted. HeLa cells were first incubated with ds(AS1411)-NPs at 4 °C for 30 min and then labeled with a Cy5-modified AS1411 (Cy5-apt). Fluorescence intensity was ultimately determined by flow cytometry. Compared with the control ds(ctrl)-NPs, the fluorescence signal from ds(AS1411)-NP-treated cells was 0.33-fold less intense (see Figure S2B in the Supporting Information). Considering the specific recognition of AS1411 to its target protein, this results suggests that the interaction between ds(AS1411)-NPs toward HeLa cells was through the nucleolin-binding and internalization pathway.

To investigate the photo-, chemo-, and combined therapeutic efficacy of these drug-loaded ds(AS1411)-NP conjugates, HeLa

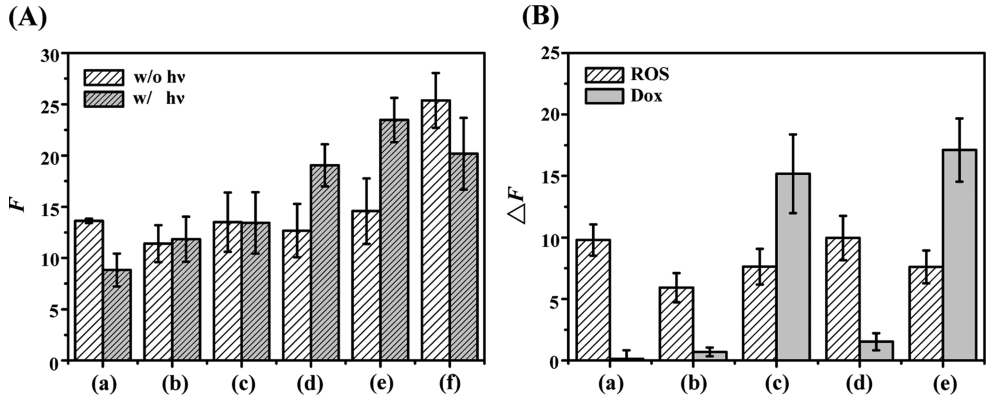

Figure 3. (A) Flow cytometry analysis of the production of reactive oxygen species (ROS) in (a) nontreated HeLa cells, and cells treated with 4× (b) ds-NPs, (c) D:ds-NPs, (d) T:ds-NPs, (e) T/D:ds-NPs, and (f) H_2O_2 (300 μM, 2h). After incubation in culture medium (10% FBS) at 37 °C and 5% CO_2 for 4 h, DCFH-DA (50 μM, 40 min) was added to each cell suspension, followed by red light exposure (632 nm, 50 min). (B) Increased intracellular ROS and Dox signals (ΔF) induced by H_2O_2. Nontreated and treated cells under different conditions were exposed to 300 μM H_2O_2 for 2 h. DCFH-DA was used to quantify the intracellular ROS production.

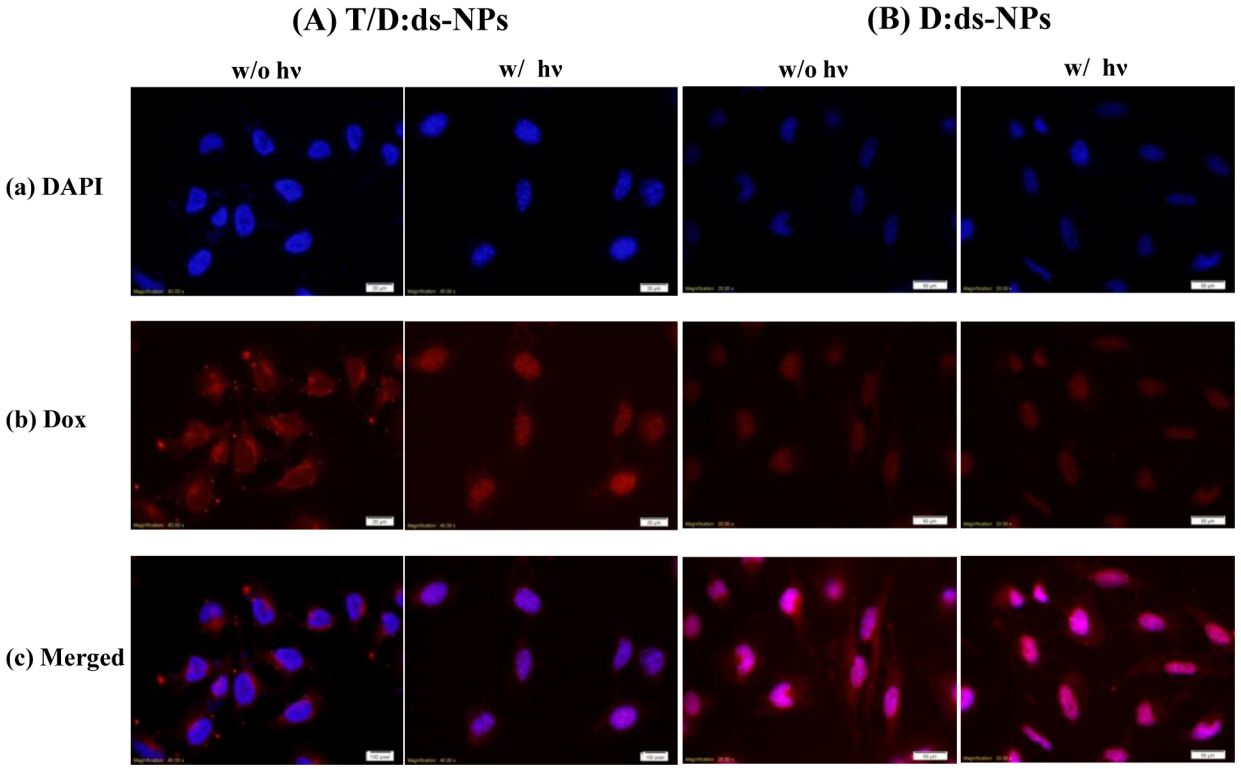

Figure 4. Fluorescence images of HeLa cells incubated with 2× (A) T/D:ds-NPs and (B) D:ds-NPs. After incubation in washing buffer (1% BSA) at 37 °C for 1 h, cells were rinsed with DPBS, followed by red light irradiation (632 nm, 30 min). For microscopic analysis, cells were fixed with 4% paraformaldehyde solution for 5 min and stained with 4,6-diamidino-2-phenylindole (DAPI,1.0 μM) for 5 min. The fluorescence images were monitored for (a) nucleus (DAPI), (b) Dox, and (c) overlay of these two channels. $TMPyP_4$ does not exhibit detectable fluorescence signals in these channels. The scale length of each image is 20 μm.

cells were incubated with T:ds-NPs and T/D:ds-NPs, respectively. After removal of the excess reagents, cells were irradiated with a red light (632 nm, 15 mW/cm^2) generated from a halogen lamp after passing through a bandpass filter with a center wavelength of 632 nm for serial time periods. Fresh medium (10% FBS) was added for further cell growth (24 h). The relative viability of cells with different treatments was then determined by performing the 3-(4,5-dimethylthiazol-2-yl)-5-(3-carboxymethoxyphenyl)-2-(4-sulfophenyl)-2H-tetrazolium) (MTT) assay. As depicted in Figure 2A, no or little cytotoxicity was observed for T:ds-NPs-treated cells before light exposure. Viability began to decline to approximately 82.4 ± 7.0% after 10 min irradiation, and decreased to around 51.0 ± 11.0% after 40 min light illumination because of the excitation of the photosensitizer, leading to the photodynamic killing of cancer cells. The cell killing activity of co-drug delivery using T/D:ds-NPs was further assessed in HeLa cells. A dramatic increase in cell death was observed depending on the light exposure time. Approximately 74.0 ± 4.2% of cells were dead when T/D:ds-NPs attached HeLa cells were irradiated with red light for 10 min. The superior cytotoxicity of T/D:ds-NPs compared with that of T:ds-NPs for all

irradiation periods suggested that a synergistic effect was involved in the cellular death.

To further confirm the combined therapeutic efficacy, cells were incubated with serial concentrations of D:ds-NPs, T:ds-NPs, and T/D:ds-NPs (Figure 2B). Compared with the cells without drug and light treatment, the increase of T:ds-NPs concentration lead to a higher cell death following a red light exposure. The cell viability of cells incubated with 4× T:ds-NPs was 64.4 ± 5.2% after 20 min irradiation. The control cells, which were incubated with ds-Au NPs, showed no cellular damage under the same illumination condition (data not shown). In addition, the dose-dependent survival curve for D:ds-NPs-treated cells was also examined. Dox-loaded ds-NPs exhibited less potent antiproliferative properties than T/D:ds-NPs at equal Dox concentration. Only 17.1 ± 2.9% of HeLa cells were killed by D:ds-NPs (4×) after light exposure for 20 min. However, an obvious loss of cell viability (21.4 ± 4.3%) had been observed for T/D:ds-NP conjugates under the same experimental condition. Collectively, the therapeutic efficacy of T/D:ds-NPs significantly improved to 2.5- and 4.6-fold compared to PDT and chemotherapy alone, indicating a synergistic enhancement of cancer therapy via the combination of photo- and chemocytotoxic reactions. It should also be noted that red light exposure showed no harm to cells without photosensitizers. The cell viability of (D:ds-NPs)-treated HeLa cells was light-independent with irradiation less than 1 h (data not shown).

To account for the different cytotoxicity of these drug nanocarriers, the intracellular ROS formation was studied using 2′,7′-dichlorodihydrofluorescein diacetate (DCFH-DA) as a probe during the combined and single treatment.[50] The cells, which were incubated with different drug conjugates, were irradiated to allow the production of significant amounts of ROS by the photosensitizer. Our experimental results (Figure 3A) clearly show that the elevated ROS was generated in both T:ds-NPs (1.5-fold, d)- and T/D:ds-NPs (1.6-fold, e)-treated cells following 50 min irradiation. However, no production of ROS was expected for cells incubated with nanoconjugates lacking photoactivated drugs (a−c) after light exposure. In addition, hydrogen peroxide (H_2O_2; 300 μM, f) was used as a positive control to stimulate intracellular ROS accumulation. An obvious fluorescence change was found in the treated cells, which was 1.5-fold higher than that without H_2O_2 (a). In contrast, subsequent exposure of the same cells to a red light leads to a decrease in the fluorescence level. The signal decay due to light illumination (column f of Figure 3A) suggested a possible photobleaching reaction of DCFH-DA under continuous irradiation. The same phenomenon was also observed in nontreated cells (a) after light exposure. Collectively, the cell death following exposure to the red light could be attributed to the accumulation of intracellular ROS induced by $TMPyP_4$-containing nanocarriers.

Further, to investigate the mechanism of the therapeutic synergism elicited by the combination of $TMPyP_4$ and Dox against HeLa cells, we monitored the intracellular signal of Dox molecules during the PDT process. As shown in Figure 4A, the fluorescence of Dox was primarily detected around the nucleus, possibly through an endolysosomal pathway after the incubation of cells with T/D:ds-NPs for 1 h. When exposed to the red light, the fluorescence emitted from Dox molecules was visible across the nucleus and predominantly colocalized with the 4, 6-diamidino-2-phenylindole (DAPI) staining. The change in the intracellular distribution of Dox in the presence of scattered light arising from Au NPs remained unchanged, implying that the intracellular release of drug payloads from T/D:ds-NPs could be triggered by red light exposure. In contrast, the fluorescence signal from cells treated with D:ds-NPs was mostly accumulated in the nucleus following cellular uptake and no change was observed after light exposure (Figure 4B). The accumulation of Dox molecules in the nucleus is likely attributable to the noncontrollable release of drugs from the complexes by diffusion or through degradation of the AS1411 aptamer inside the cells. The obvious signal difference between HeLa cells incubated with T/D:ds-NPs and D:ds-NPs before light exposure suggested that the incorporation of $TMPyP_4$ into the G-quadruplex structures of these aptamer-tethered nanoconjugates effectively trapped guest molecules. According to the flow cytometric analysis, less intense fluorescence signals (29.9 au) were detected from cells incubated with T/D:ds-NPs than those detected in D:ds-NPs-treated cells (43.9 au). Because the fluorescence intensity of Dox was largely quenched by Au NPs, the recovery of Dox signals could be directly correlated to the release of Dox inside the cells. Additionally, results obtained by AAS exhibited similar uptake efficiency of both nanoconjugates toward HeLa cells (data not shown). Collectively, these results confirmed a unique "gate keeper" property of $TMPyP_4$ molecules in our developed nanoplatform. Furthermore, upon light illumination, the capping effect was removed, thus allowing a subsequent release of the entrapped cargos, as evidenced by the significant change in fluorescence distribution inside the cells. Although the ROS generated by the photoactive compound could lead to endolysosomal membrane damage, the rapid transfer of small drug molecules from the endolysosome to the nucleus during illumination is consistent with the data previously reported.[51−53]

From the intracellular analysis, it was quite evident that Dox molecules could be liberated from the $TMPyP_4$-loaded nanoconjugates under light irradiation. However, only a slight increase in the fluorescence signal inside the treated HeLa cells after illumination was examined by flow cytometry (data not shown). One possible explanation for the limited intensity change is due to the photochemical destruction of drug molecules during irradiation.[54,55] In addition, the occurrence of oxidative reactions through the ROS also results in the decline of the fluorescence signal.[56] Among the ROS, H_2O_2 is a less effective oxidant than singlet oxygen ($^1O_2$) and other free radicals such as superoxide anion ($O_2^{\bullet-}$), and hydroxyl radical ($\cdot OH$).[57,58] Therefore, we tested the ability of H_2O_2 to induce Dox release inside the cells. HeLa cells were incubated with different nanoconjuagtes at the same Au NP concentration (4 ×) for 4 h. Cells were then carefully washed to remove unbound drugs and reincubated with H_2O_2 (300 μM) for 2 h. Flow cytometry data (Figure 3B) revealed an apparent increase of Dox fluorescence in both D:ds-NPs- and T/D:ds-NPs-treated cells (c and e), whereas the others remained almost unchanged. The elevation of intracellular ROS levels was also assessed using DCFH-DA, with the resulting fluorescence showing no significant difference between the study groups. Here, the results supported the indication that the release of Dox from the T/D:ds-NP nanocomposites could be triggered by an external red light, likely due to the production of significant amounts of ROS.

It is widely accepted that ROS can attack DNA primarily through the reaction of guanine residues in DNA fragments. Oxidative DNA damage, which results in base mispairings, strand breaks, and DNA cleavage, is considered as the major

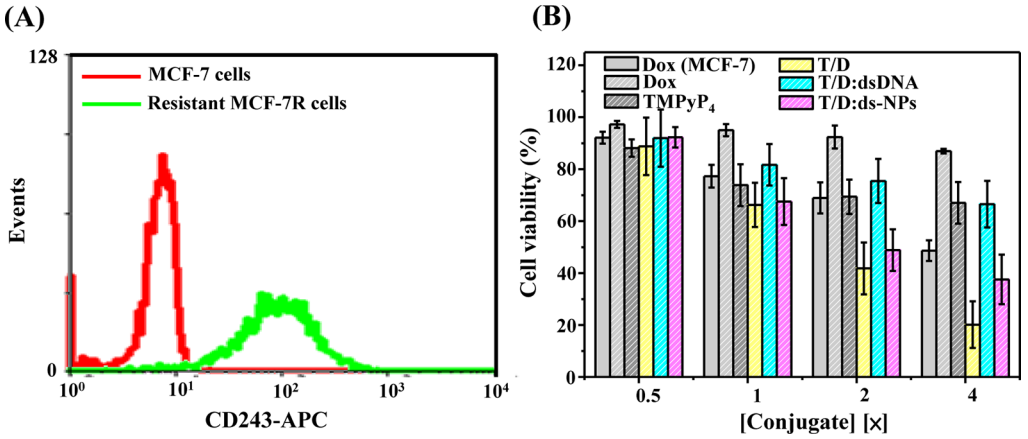

Figure 5. (A) Flow cytometry assay for the binding of the UIC2 antibody in (a) MCF-7 cells and (b) resistant MCF-7R cells. (B) MTT assay of MCF-7 cells (Dox only) and resistant MCF-7R cells incubated with Dox, $TMPyP_4$, $TMPyP_4$/Dox (T/D), T/D:dsDNA, and T/D:ds-NPs in washing buffer (1% BSA) at 37 °C and 5% CO_2 for 4 h. After drug treatments, cells were exposed to red light irradiation (632 nm) for 20 min and subsequently grown in fresh medium (10% FBS) for 24 h. The drug concentration of Dox and $TMPyP_4$ denoted as 1× corresponds to 3.6 and 3.9 μM, respectively.

cause of cancer.[59−61] Moreover, cationic porphyrins, which possess strong binding affinity for nucleic acids, have attracted considerable attention as effective photodynamic sensitizers. They can achieve effective DNA photocleavage by light irradiation.[62,63] To confirm that the photoresponsive Dox release is attributable to the PDT process, the photoinduced DNA cleavage activity of T:ds-NPs exposed to red light was studied by agarose gel electrophoresis in 0.5× TBE buffer. The electrophorogram given in Figure S3A (see the Supporting Information) shows that the T:ds-NP conjugate (Lane b) moves faster than the T:ds-NP conjugate without light treatment (Lane a). Because the surface charges of the $TMPyP_4$-loaded ds-NPs remain unchanged following light illumination (data not shown), the slight increase in electrophoretic mobility indicated a small reduction in hydrodynamic diameter. This result is in contrast to that obtained for the ds-NPs without $TMPyP_4$ because no apparent shift in the electrophorogram was observed under a similar irradiation condition (Lane c and d). In addition, dynamic light-scattering (DLS) measurements (see Figure S3B in the Supporting Information) showed that the size of T:ds-NPs decreased from 54.6 ± 1.9 nm to 43.9 ± 2.0 nm with light illumination, whereas the size of ds-NPs decreased from 44.6 ± 2.0 nm to 41.5 ± 3.1, respectively. This result correlates with the considerable increase of DNA signal from the supernatant of T:ds-NPs compared with that of ds-NPs (see Figure S3C in the Supporting Information). After exposure to visible light, the supernatants of the sample solution were isolated by centrifugation. The photoinduced DNA cleavage was quantified using OliGreen fluorescent stain. When exposed to 20 min irradiation, approximately 2.8-fold enhanced fluorescence signal was obtained from T:ds-NPs, whereas ds-NPs showed limited increase (1.5-fold). Collectively, the ROS-mediated DNA cleavage induced by photoactivation of $TMPyP_4$ provides possibilities for payload release from the double-strand structures of DNA molecules.

Recent studies have suggested that photosensitizers could overcome the problems associated with P-glycoprotein (P-gp)-mediated drug efflux, resulting in high photodynamic activity against multidrug resistant (MDR) cells.[41] On the basis of these properties, we tested our constructed drug delivery platform in MDR-MCF7 cells (MCF-7R), which shows high expression level of nucleolin.[49] In addition, the up-regulation of P-gp on the surface of drug-resistant cell lines was also examined by flow cytometry analysis. A high florescence intensity of APC-conjugated anti-P-gp antibody[64] was observed in MCF-7R cells compared to that in MCF-7 cells (Figure 5A), indicating approximately 12-fold up-regulation of P-gp in MCF-7R cells compared to MCF-7 cells. MCF-7R cells were then incubated with different drug-loaded conjugates at serial concentrations followed by red light illumination for 20 min. The high proliferation rate (second column of Figure 5B) suggested a less pronounced cytotoxic effect of free Dox toward drug-resistant MCF-7R cells compared with MCF-7 cells (first column). However, cellular viability declined when MCF-7R cells were treated with $TMPyP_4$ and then irradiated. This result confirmed that the drug-resistant cells were more susceptible to PDT-induced cellular damage as reported. Moreover, in comparison with PDT treatment alone, codelivery of $TMPyP_4$/Dox (T/D) displayed a greater potency to MCF-7R cells. This result is consistent with previous findings that the photosensitizer-mediated membrane disruption can greatly improve the anticancer efficacy of chemo drugs by overcoming the MDR of cancer cells.[51,53] The killing efficiency was further investigated by simultaneous delivery of T/D by applying ds-NPs to the MDR tumor cells. Although the cytotoxic effect of T/D:ds-NPs was similar or slightly less toxic than that of free T/D (Figure 5B), severe side effects on normal tissues could be minimized by tumor-targeted delivery through the formulation of aptamer-conjugated nanoplatform. Moreover, the cytotoxicity to MCF-7R cells in response to the codelivery of $TMPyP_4$ and Dox was also confirmed by using the G-quadruplex structure (dsAS1411) as a drug carrier. The physically conjugated drug:apt complex exhibited high stability and was an ideal vector for nucleolin targeting and drug delivery.[48] In contrast to the dramatic cytotoxic effect of our T/D:ds-NPs, the killing efficacy of T/D:dsDNA complex toward MCF-7R cells was significantly less pronounced. This result suggests that nanoscale carriers, which can achieve sufficient drug accumulation via endocytic uptake on the cellular level and promote responsive intracellular drug release, can deliver chemotherapeutic drugs to overcome MDR.

EXPERIMENTAL DETAILS

Chemicals. Gold(III) chloride hydrate, tris, doxorubicin hydrochloride, 6-mercapto-1-hexanol, (97%), trisodium citrate 2-hydrate, sodium dodecyl sulfate (SDS), sodium chloride, and 5,10,15,20-tetrakis(1-methylpyridinium 4-yl)porphyrin ($TMPyP_4$) were obtained from Sigma–Aldrich (St. Louis, MO, USA). Fetal bovine serum and penicillin/streptomycin were obtained from GIBCO (Grand Island, NY, USA). Dulbecco's phosphate-buffered saline was purchased from Biosource (Camarillo, CA, USA). The 5′-thiol-modified aptamer, ds(AS1411) (strand 1:5′-thiol-TTT TTT TTT TTC GAT CGT CGA TCG TCG ATC G)-3′, strand 2:5′-GGT GGT GGT GGT TGT GGT GGT GGT GGT TTT TTC GAT CGA CGA TCG ACG ATC GA-3′), was purchased from Integrated DNA Technology Incorporated (Coralville, IA, USA). Deionized water (18.2 MΩ cm) was used to prepare all of the aqueous solutions. For the cellular experiments, all of the reagents, buffers, and culture medium were sterilized by steam autoclave (121 °C, 40 min) or filtration (0.22 μm pore size, Millipore), and maintained under a sterile condition.

Synthesis of Au NPs. Thirteen nanometer Au NPs were synthesized according to the method developed by Frens.[65] Briefly, 0.1 mL of 1.0 M chloroauric acid was added to 100 mL of deionized water, and the solution boiled. Next, 1.0 mL of 0.4 M trisodium citrate was added to the solution to obtain 12.6 (±0.8)-nm Au NPs. The sizes and absorption spectra of Au NPs were verified using a Hitachi H-7100 transmission electron microscope (Tokyo, Japan) and a Cary 100 UV–Vis spectrophotometer (Varian, Palo Alto, CA, USA). The concentration of Au NPs in each aliquot was also determined by UV–Vis spectrophotometric measurements via Beer's law ($A = \varepsilon bc$).[66] The concentration of the as-prepared Au NP is denoted as 1×, which corresponds to the concentration of approximately 13 nM.

Synthesis of Drug-Loaded ds(AS1411)-Au NPs. To stabilize Au NPs during the conjugation, we added 10% SDS (5 μL) into 0.5 mL of Au NPs (1 ×) for 24 h. Twenty micromolar ds(AS1411) was first heated at 95 °C for 5 min and gradually anneal to room temperature in 28 mM Tris-acetate buffer (pH 7.2), containing 0.1 M NaCl, 0.1 M KCl, and 4.0 mM $MgCl_2$. The ds(AS1411) solution was then added into an aqueous Au NP solution (0.1% SDS and 0.06 M NaCl in 10 mM phosphate buffer, pH 7.0) to obtain the resulting conjugates, ds-NPs. After reaction for 1 h, 0.5 M NaCl (in 10 mM phosphate, pH 7.0) was added to bring the salt concentration to 0.1 M. This solution was incubated for an additional 12 h. Next, the mixture was equilibrated with 4 μM 6-mercaptohexanol for 30 min and centrifuged at 13 000 rpm for 20 min to remove excess dsDNA. DNA conjugated-NPs were then resuspended in phosphate-buffered saline (PBS, 0.1 M NaCl). For drug loading, Dox (4 μM) and/or $TMPyP_4$ (4 μM) was subsequently added into the solution of ds-NPs (1 ×). Following 2 h incubation, the mixture was subjected to two centrifuge/wash cycles (13 000 rpm, 20 min) to remove excess drug and resuspended in 1% BSA containing washing buffer [4.5 g/L glucose and 5 mM $MgCl_2$ in Dulbecco's PBS with calcium chloride and magnesium chloride (Sigma–Aldrich)]. The amount of unbound drug molecules in the supernatant was calculated from the emission intensity of Dox at 596 nm (excitation at 480 nm) and $TMPyP_4$ at 715 nm (excitation at 432 nm), respectively.

Characterization of DNA Loading. The loading of DNA onto the Au NP surface was determined by fluorescence measurement (Tecan Safire Plate Reader, Tecan Group AG, Basel, Switzerland) of fluorescein-labeled DNA (strand 2). The fluorescence maxima (measured at 520 nm) of the supernatant, containing free DNA removed from the particle, were converted to molar concentrations of fluorescein-modified DNA by interpolation from a standard linear calibration curve. Standard curves were prepared with known concentrations of fluorescein-labeled DNA using identical buffer pH and salt concentrations. Finally, the mean number of DNA per particle was obtained by dividing the measured DNA molar concentration by the original Au NP concentration.

Cell Lines and Buffers. HeLa cells (ATCC CCL-2 human cervical carcinoma) and MCF-7 (HTB-22 breast adenocarcinoma) was obtained from American Type Culture Collection (ATCC, Manassas, VA, USA). The resistant cell line MCF-7R to adriamycin was kindly provided by Professor Chi-Shiun Chiang, National Tsing Hua University, Taiwan. All the cells were cultured in suspension in DMEM medium supplemented with 10% FBS and 1% penicillin-streptomycin (Invitrogen, Carlsbad, CA, USA) at 37° in a balanced air humidified incubator with an atmosphere of 5% CO_2. Cell density was determined using a hemocytometer, and this was done before experimentation. All experiments were performed on cells passaged 12 h prior.

Dark-Field and Fluorescence Microscopic Analyses. To observe cellular uptake, we seeded HeLa cells at a density of 1.0×10^5 cells per well on 10 × 10 mm sterile cover glasses inserted into 48-well plates for 12 h. The culture medium was replaced with washing buffer (1% BSA) containing Dox (2 μM), D:ds-NPs (2×) and T/D:ds-NPs (2×), respectively. After 1 h incubation, the cells were rinsed with DPBS twice, fixed with 4% paraformaldehyde solution for 5 min. Cover glasses were then placed on the slide glasses. The scattering light of Au NP conjugates inside HeLa cells was recorded using an inverted microscope (Olympus IX71) with a highly numerical aperture dark-field condenser (U-DCW, Olympus). The Internalization of Dox and $TMPyP_4$ into live cells was monitored by fluorescence using an inverted fluorescence microscope. Nuclei were visualized after staining with 4′,6-diamidino-2-phenylindole (DAPI, 1.0 μM) for 5 min.

Intracellular Reactive Oxygen Species Generation by Red Light Irradiation. Intracellular ROS generation was determined by the increase in fluorescence due to DCFH-DA oxidation. HeLa cells were seeded at a density of 2×10^4 cells per well into 96-well plates for 12 h. The culture medium was replaced with complete culture medium containing ds-NPs (4×), D:ds-NPs (4×), T:ds-NPs (4×) and T/D:ds-NPs (4×), respectively. Following 4 h incubation, the cells were washed twice in washing buffer (1% BSA). 50 μM DCFH-DA (Molecular Probes) prepared in serum-free DMEM medium was added to the cells for 40 min at 37 °C. The cells were then divided into two groups under different conditions: (1) no irradiation, and (2) irradiation for 50 min using a 632 nm light (15 mW/cm^2). To compare intracellular ROS levels, H_2O_2 (300 μM, 2 h)-treated cells were used as a positive control. Finally, cells were trypsinized and collected in the tube by centrifugation (980 g, 5 min) and resuspended in 200 μL DPBS for flow cytometry analysis with excitation and emission settings of 488 and 530 nm, respectively. For each analysis, at least 10 000 events were counted.

Intracellular Drug Release Based on ROS Generation. To observe intracellular Dox release, HeLa cells were grown in a 96-well culture plate of 1.0×10^5 cells per well for 12 h. Cells were treated with different conjugates (4× ds-NPs, D:ds-NPs, T:ds-NPs, and T/D:ds-NPs) prepared in complete culture medium for 4 h, respectively. Excess conjugates were then replaced by washing buffer supplemented with 1% BSA. To increase the intracellular ROS level, treated cells were incubated with 300 μM H_2O_2 for 2 h. The triggered drug release process was further observed by flow cytometric analysis to monitor Dox fluorescence.

Cytotoxicity Assay. HeLa, MCF-7 and MCF-7R cells were seeded into 96-well plate (8×10^3 cells per well) for 12 h. The cells were washed once and incubated with various concentration of different drug conjugates (Dox, $TMPyP_4$, T/D, T:ds-NPs, D:ds-NPs, T/D:dsDNA, and T/D:ds-NPs) at 37 °C, respectively. Following 4 h treatment, the well contents not specifically bound or taken-up by the cells were removed by rinsing the cells twice in washing buffer (1% BSA). One group of the treated cells was kept in the dark, while the other was exposure to a 632 nm red light (15 mW/cm^2) for 20 min. After irradiation, the cells were kept in complete culture medium for an additional growth at 37 °C in a 5% CO_2 atmosphere for 24 h. For cytotoxicity measurement, 10 μL Cell Titer reagent (Promega, Madison, WI, USA) was added to each well and incubated for 2 h. Using a plate reader, the absorption was recorded at 570 and 600 nm, respectively. The percentage of cell viability was determined by comparing cells treated with drug conjugates with the untreated control.

CONCLUSIONS

In conclusion, Au NPs assembled with a nucleolin-bound aptamer-incorporated DNA motif was constructed as an effective nanocarrier for co-drug delivery. When exposed to visible light, the photodynamic action induced by the photoactivated sensitizers produced abundant ROS. The DNA moiety, which serves as a molecular switch of these drug nanocarriers, scavenges a number of ROS, thus driving the specific release of complementary drug molecules intercalated into the dsDNA onto the Au NP surfaces. The combination of PDT and chemotherapy leads to an improvement in the therapeutic inhibition of tumor cell growth over individual treatment. Moreover, this nanoscale delivery system is immensely advantageous in combatting tumor drug resistance with effective intracellular transport as well as optimal antitumor efficacy.

ASSOCIATED CONTENT

Supporting Information

Co-drug loading analysis, microscopic and flow cytometric assay, photoirradiation effects on aptamer-modified Au NPs. This material is available free of charge via the Internet at http://pubs.acs.org.

AUTHOR INFORMATION

Corresponding Author

*E-mail: yufen@mx.nthu.edu.tw.

Author Contributions

The manuscript was written through contributions of all authors. All authors have given approval to the final version of the manuscript.

Notes

The authors declare no competing financial interest.

ACKNOWLEDGMENTS

This work was supported by National Tsing Hua University (101N7046E1) and the Ministry of Science and Technology (NSC 102-2113-M-007-005-MY3, NSC 102-2627-M-007-004) of Taiwan, ROC.

REFERENCES

(1) Panjehpour, M.; Overholt, B. F.; Haydek, J. M.; Lee, S. G. Results of Photodynamic Therapy for Ablation of Dysplasia and Early Cancer in Barrett's Esophagus and Effect of Oral Steroids on Stricture Formation. *Am. J. Gastroenterol.* **2000**, *95*, 2177−2184.

(2) Varma, S.; Wilson, H.; Kurwa, H. A.; Gambles, B.; Charman, C.; Pearse, A. D.; Taylor, D.; Anstey, A. V. Bowen's Disease, Solar Keratoses and Superficial Basal Cell Carcinomas Treated by Photodynamic Therapy Using a Large-Field Incoherent Light Source. *Br. J. Dermatol.* **2001**, *144*, 567−574.

(3) Rigual, N. R.; Thankappan, K.; Cooper, M.; Sullivan, M. A.; Dougherty, T.; Popat, S. R.; Loree, T. R.; Biel, M. A.; Henderson, B. Photodynamic Therapy for Head and Neck Dysplasia and Cancer. *Arch. Otolaryngol. Head Neck Surg.* **2009**, *135*, 784−788.

(4) Dougherty, T. J.; Gomer, C. J.; Henderson, B. W.; Jori, G.; Kessel, D.; Korbelik, M.; Moan, J.; Peng, Q. Photodynamic Therapy. *J. Natl. Cancer Inst.* **1998**, *90*, 889−905.

(5) Brown, S. B.; Brown, E. A.; Walker, I. The Present and Future Role of Photodynamic Therapy in Cancer Treatment. *Lancet Oncol.* **2004**, *5*, 497−508.

(6) Triesscheijn, M.; Baas, P.; Schellens, J. H.; Stewart, F. A. Photodynamic Therapy in Oncology. *Oncologist* **2006**, *11*, 1034−1044.

(7) O'Connor, A. E.; Gallagher, W. M.; Byrne, A. T. Porphyrin and Nonporphyrin Photosensitizers in Oncology: Preclinical and Clinical Advances in Photodynamic Therapy. *Photochem. Photobiol.* **2009**, *85*, 1053−1074.

(8) Ethirajan, M.; Chen, Y.; Joshi, P.; Pandey, R. K. The Role of Porphyrin Chemistry in Tumor Imaging and Photodynamic Therapy. *Chem. Soc. Rev.* **2011**, *40*, 340−362.

(9) Bechet, D.; Couleaud, P.; Frochot, C.; Viriot, M. L.; Guillemin, F.; Barberi-Heyob, M. Nanoparticles as Vehicles for Delivery of Photodynamic Therapy Agents. *Trends Biotechnol.* **2008**, *26*, 612−621.

(10) Chatterjee, D. K.; Fong, L. S.; Zhang, Y. Nanoparticles in Photodynamic Therapy: an Emerging Paradigm. *Adv. Drug Delivery Rev.* **2008**, *60*, 1627−1637.

(11) Wilson, B. C.; Patterson, M. S. The Physics, Biophysics and Technology of Photodynamic Therapy. *Phys. Med. Biol.* **2008**, *53*, R61−R109.

(12) Master, A.; Livingston, M.; Sen Gupta, A. Photodynamic Nanomedicine in the Treatment of Solid Tumors: Perspectives and Challenges. *J. Controlled Release* **2013**, *168*, 88−102.

(13) Manthe, R. L.; Foy, S. P.; Krishnamurthy, N.; Sharma, B.; Labhasetwar, V. Tumor Ablation and Nanotechnology. *Mol. Pharm.* **2010**, *7*, 1880−1898.

(14) Roy, I.; Ohulchanskyy, T. Y.; Pudavar, H. E.; Bergey, E. J.; Oseroff, A. R.; Morgan, J.; Dougherty, T. J.; Prasad, P. N. Ceramic-Based Nanoparticles Entrapping Water-Insoluble Photosensitizing Anticancer Drugs: a Novel Drug−Carrier System for Photodynamic Therapy. *J. Am. Chem. Soc.* **2003**, *125*, 7860−7865.

(15) Tang, W.; Xu, H.; Kopelman, R.; Philbert, M. A. Photodynamic Characterization and in Vitro Application of Methylene Blue-Containing Nanoparticle Platforms. *Photochem. Photobiol.* **2005**, *81*, 242−249.

(16) Wieder, M. E.; Hone, D. C.; Cook, M. J.; Handsley, M. M.; Gavrilovic, J.; Russell, D. A. Intracellular Photodynamic Therapy with Photosensitizer-Nanoparticle Conjugates: Cancer Therapy Using a 'Trojan Horse'. *Photochem. Photobiol. Sci.* **2006**, *5*, 727−734.

(17) Cheng, Y.; Samia, A. C.; Meyers, J. D.; Panagopoulos, I.; Fei, B. W.; Burda, C. Highly Efficient Drug Delivery with Gold Nanoparticle Vectors for in Vivo Photodynamic Therapy of Cancer. *J. Am. Chem. Soc.* **2008**, *130*, 10643−10647.

(18) Zhang, M.; Murakami, T.; Ajima, K.; Tsuchida, K.; Sandanayaka, A. S. D.; Ito, O.; Iijima, S.; Yudasaka, M. Fabrication of ZnPc/Protein Nanohorns for Double Photodynamic and Hyperthermic Cancer Phototherapy. *Proc. Natl. Acad. Sci. U.S.A.* **2008**, *105*, 14773−14778.

(19) Khdair, A.; Gerard, B.; Handa, H.; Mao, G. Z.; Shekhar, M. P. V.; Panyam, J. Surfactant-Polymer Nanoparticles Enhance the Effectiveness of Anticancer Photodynamic Therapy. *Mol. Pharm.* **2008**, *5*, 795−807.

(20) Rossi, L. M.; Silva, P. R.; Vono, L. L. R.; Fernandes, A. U.; Tada, D. B.; Baptista, M. S. Protoporphyrin IX Nanoparticle Carrier: Preparation, Optical Properties, and Singlet Oxygen Generation. *Langmuir* **2008**, *24*, 12534−12538.

(21) Camerin, M.; Magaraggia, M.; Soncin, M.; Jori, G.; Moreno, M.; Chambrier, I.; Cook, M. J.; Russell, D. A. The in Vivo Efficacy of Phthalocyanine-Nanoparticle Conjugates for the Photodynamic Therapy of Amelanotic Melanoma. *Eur. J. Cancer* **2010**, *46*, 1910−1918.

(22) McCarthy, J. R.; Korngold, E.; Weissleder, R.; Jaffer, F. A. A Light-Activated Theranostic Nanoagent for Targeted Macrophage Ablation in Inflammatory Atherosclerosis. *Small* **2010**, *6*, 2041−2049.

(23) Koo, H.; Lee, H.; Lee, S.; Min, K. H.; Kim, M. S.; Lee, D. S.; Choi, Y.; Kwon, I. C.; Kim, K.; Jeong, S. Y. In Vivo Tumor Diagnosis and Photodynamic Therapy via Tumoral pH-Responsive Polymeric Micelles. *Chem. Commun.* **2010**, *46*, 5668−5670.

(24) Couleaud, P.; Morosini, V.; Frochot, C.; Richeter, S.; Raehm, L.; Durand, J.-O. Silica-Based Nanoparticles for Photodynamic Therapy Applications. *Nanoscale* **2010**, *2*, 1083−1095.

(25) Lee, S. J.; Koo, H.; Lee, D. E.; Min, S.; Lee, S.; Chen, X.; Choi, Y.; Leary, J. F.; Park, K.; Jeong, S. Y.; Kwon, I. C.; Kim, K.; Choi, K. Tumor-Homing Photosensitizer-Conjugated Glycol Chitosan Nanoparticles for Synchronous Photodynamic Imaging and Therapy Based on Cellular On/Off System. *Biomaterials* **2011**, *32*, 4021−4029.

(26) Jin, C. S.; Zheng, G. Liposomal Nanostructures for Photosensitizer Delivery. *Lasers Surg. Med.* **2011**, *43*, 734−748.
(27) Xiao, L.; Gu, L.; Howell, S. B.; Sailor, M. J. Porous Silicon Nanoparticle Photosensitizers for Singlet Oxygen and Their Phototoxicity against Cancer Cells. *ACS Nano* **2011**, *5*, 3651−3659.
(28) Yoon, H. Y.; Koo, H.; Choi, K. Y.; Lee, S. J.; Kim, K.; Kwon, I. C.; Leary, J. F.; Park, K.; Yuk, S. H.; Park, J. H.; Choi, K. Tumor-Targeting Hyaluronic Acid Nanoparticles for Photodynamic Imaging and Therapy. *Biomaterials* **2012**, *33*, 3980−3989.
(29) Khaing Oo, M. K.; Yang, Y.; Hu, Y.; Gomez, M.; Du, H.; Wang, H. Gold Nanoparticle-Enhanced and Size-Dependent Generation of Reactive Oxygen Species from Protoporphyrin IX. *ACS Nano* **2012**, *6*, 1939−1947.
(30) Zhang, P.; Steelant, W.; Kumar, M.; Scholfield, M. Versatile Photosensitizers for Photodynamic Therapy at Infrared Excitation. *J. Am. Chem. Soc.* **2007**, *129*, 4526−4527.
(31) Shan, J. N.; Budijono, S. J.; Hu, G. H.; Yao, N.; Kang, Y. B.; Ju, Y. G.; Prud'homme, R. K. Pegylated Composite Nanoparticles Containing Upconverting Phosphors and Meso-Tetraphenyl porphine (TPP) for Photodynamic Therapy. *Adv. Funct. Mater.* **2011**, *21*, 2488−2495.
(32) Idris, N. M.; Gnanasammandhan, M. K.; Zhang, J.; Ho, P. C.; Mahendran, R.; Zhang, Y. In vivo Photodynamic Therapy Using Upconversion Nanoparticles as Remote-Controlled Nanotransducers. *Nat. Med.* **2012**, *18*, 1580−1585.
(33) Wang, C.; Cheng, L.; Liu, Z. Upconversion Nanoparticles for Photodynamic Therapy and Other Cancer Therapeutics. *Theranostics* **2013**, *3*, 317−330.
(34) Delehanty, J. B.; Boeneman, K.; Bradburne, C. E.; Robertson, K.; Medintz, I. L. Quantum Dots: a Powerful Tool for Understanding the Intricacies of Nanoparticle-Mediated Drug Delivery. *Expert Opin. Drug Delivery* **2009**, *6*, 1091−1112.
(35) Rai, P.; Mallidi, S.; Zheng, X.; Rahmanzadeh, R.; Mir, Y.; Elrington, S.; Khurshid, A.; Hasan, T. Development and Applications of Photo-Triggered Theranostic Agents. *Adv. Drug Delivery Rev.* **2010**, *62*, 1094−124.
(36) Huang, P.; Li, Z. M.; Lin, J.; Yang, D. P.; Gao, G.; Xu, C.; Bao, L.; Zhang, C. L.; Wang, K.; Song, H.; Hu, H. Y.; Cui, D. X. Photosensitizer-Conjugated Magnetic Nanoparticles for in Vivo Simultaneous Magnetofluorescent Imaging and Targeting Therapy. *Biomaterials* **2011**, *32*, 3447−3458.
(37) Peterson, C. M.; Lu, J. M.; Sun, Y.; Peterson, C. A.; Shiah, J. G.; Straight, R. C.; Kopecek, J. Combination Chemotherapy and Photodynamic Therapy with N-(2-hydroxypropyl) Methacrylamide Copolymer-Bound Anticancer Drugs Inhibit Human Ovarian Carcinoma Heterotransplanted in Nude Mice. *Cancer Res.* **1996**, *56*, 3980−3985.
(38) Hongrapipat, J.; Kopeckova, P.; Liu, J.; Prakongpan, S.; Kopecek, J. Combination Chemotherapy and Photodynamic Therapy with Fab'Fragment Targeted HPMA Copolymer Conjugates in Human Ovarian Carcinoma Cells. *Mol. Pharm.* **2008**, *5*, 696−709.
(39) Peng, C. L.; Lai, P. S.; Lin, F. H.; Yueh-Hsiu Wu, S.; Shieh, M. J. Dual Chemotherapy and Photodynamic Therapy in an HT-29 Human Colon Cancer Xenograft Model Using SN-38-Loaded Chlorin-Core Star Block Copolymer Micelles. *Biomaterials* **2009**, *30*, 3614−3625.
(40) Lau, J. T.; Lo, P. C.; Fong, W. P.; Ng, D. K. A Zinc(II) Phthalocyanine Conjugated with an Oxaliplatin Derivative for Dual Chemo- and Photodynamic Therapy. *J. Med. Chem.* **2012**, *55*, 5446−5454.
(41) Khdair, A.; Chen, D.; Patil, Y.; Ma, L.; Dou, Q. P.; Shekhar, M. P.; Panyam, J. Nanoparticle-Mediated Combination Chemotherapy and Photodynamic Therapy Overcomes Tumor Drug Resistance. *J. Controlled Release* **2010**, *141*, 137−144.
(42) Ruebner, A.; Yang, Z.; Leung, D.; Breslow, R. A Cyclodextrin Dimer with a Photocleavable Linker as a Possible Carrier for the Photosensitizer in Photodynamic Tumor Therapy. *Proc. Natl. Acad. Sci. U.S.A.* **1999**, *96*, 14692−14693.
(43) Baugh, S. D.; Yang, Z.; Leung, D. K.; Wilson, D. M.; Breslow, R. Cyclodextrin Dimers as Cleavable Carriers of Photodynamic Sensitizers. *J. Am. Chem. Soc.* **2001**, *123*, 12488−12494.
(44) Jiang, M. Y.; Dolphin, D. Site-Specific Prodrug Release Using Visible Light. *J. Am. Chem. Soc.* **2008**, *130*, 4236−4237.
(45) Bates, P. J.; Kahlon, J. B.; Thomas, S. D.; Trent, J. O.; Miller, D. M. Antiproliferative Activity of G-rich Oligonucleotides Correlates with Protein Binding. *J. Biol. Chem.* **1999**, *274*, 26369−26377.
(46) Kim, D.; Jeong, Y. Y.; Jon, S. A Drug-Loaded Aptamer-Gold Nanoparticle Bioconjugate for Combined CT Imaging and Therapy of Prostate Cancer. *ACS Nano* **2010**, *4*, 3689−3696.
(47) Luo, Y.-L.; Shiao, Y.-S.; Huang, Y.-F. Release of Photoactivatable Drugs from Plasmonic Nanoparticles for Targeted Cancer Therapy. *ACS Nano* **2011**, *5*, 7796−7804.
(48) Shieh, Y.-A.; Yang, S.-J.; Wei, M.-F.; Shieh, M.-J. Aptamer-Based Tumor-Targeted Drug Delivery for Photodynamic Therapy. *ACS Nano* **2010**, *4*, 1433−1442.
(49) Bates, P. J.; Laber, D. A.; Miller, D. M.; Thomas, S. D.; Trent, J. O. Discovery and Development of the G-rich Oligonucleotide AS1411 as a Novel Treatment for Cancer. *Exp. Mol. Pathol.* **2009**, *86*, 151−164.
(50) Sentürker, S.; Tschirret-Guth, R.; Morrow, J.; Levine, R.; Shacter, E. Induction of Apoptosis by Chemotherapeutic Drugs without Generation of Reactive Oxygen Species. *Arch. Biochem. Biophys.* **2002**, *397*, 262−272.
(51) Hogset, A.; Prasmickaite, L.; Selbo, P. K.; Hellum, M.; Engesaeter, B. O.; Bonsted, A.; Berg, K. Photochemical Internalisation in Drug and Gene Delivery. *Adv. Drug Delivery Rev.* **2004**, *56*, 95−115.
(52) Nishiyama, N.; Iriyama, A.; Jang, W. D.; Miyata, K.; Itaka, K.; Inoue, Y.; Takahashi, H.; Yanagi, Y.; Tamaki, Y.; Koyama, H.; Kataoka, K. Light-Induced Gene Transfer from Packaged DNA Enveloped in a Dendrimeric Photosensitizer. *Nat. Mater.* **2005**, *4*, 934−941.
(53) Lee, C. S.; Park, W.; Park, S. J.; Na, K. Endolysosomal Environment-Responsive Photodynamic Nanocarrier to Enhance Cytosolic Drug Delivery via Photosensitizer-Mediated Membrane Disruption. *Biomaterials* **2013**, *34*, 9227−9236.
(54) Wood, M. J.; Irwin, W. J.; Scott, D. K. Photodegradation of Doxorubicin, Daunorubicin and Epirubicin Measured by High-Performance Liquid Chromatography. *J. Clin. Pharm. Ther.* **1990**, *15*, 291−300.
(55) Lee, C. M.; Tannock, I. F. Inhibition of Endosomal Sequestration of Basic Anticancer Drugs: Influence on Cytotoxicity and Tissue Penetration. *Br. J. Cancer* **2006**, *94*, 863−869.
(56) Zheng, Q.; Jockusch, S.; Zhou, Z.; Blanchard, S. C. The Contribution of Reactive Oxygen Species to the Photobleaching of Organic Fluorophores. *Photochem. Photobiol.* **2014**, *90*, 448−454.
(57) Blokhina, O.; Virolainen, E.; Fagerstedt, K. V. ntioxidants, Oxidative Damage and Oxygen Deprivation Stress: a Review. *Ann. Bot.* **2003**, *91*, 179−194.
(58) Toledano, M. B.; Fourquet, S.; D'AutréauxB. In *Signal Transduction: Pathways, Mechanisms and Diseases*; Sitaramayya, A., Ed.; Springer: Berlin, 2010; Chapter 17, pp 313−336.
(59) Wiseman, H.; Halliwell, B. Damage to DNA by Reactive Oxygen and Nitrogen Species: Role in Inflammatory Disease and Progression to Cancer. *Biochem. J.* **1996**, *313*, 17−29.
(60) Kamiya, H. Mutagenic Potentials of Damaged Nucleic Acids Produced by Reactive Oxygen/Nitrogen Species: Approaches Using Synthetic Oligonucleotides and Nucleotides: Survey and Summary. *Nucleic Acids Res.* **2003**, *31*, 517−531.
(61) Waris, G.; Ahsan, H. Reactive Oxygen Species: Role in the Development of Cancer and Various Chronic Conditions. *J. Carcinog.* **2006**, *5*, 14.
(62) Tada-Oikawa, S.; Oikawa, S.; Hirayama, J.; Hirakawa, K.; Kawanishi, S. NA Damage and Apoptosis Induced by Photosensitization of 5,10,15,20-Tetrakis (N-methyl-4-pyridyl)-21H,23H-porphyrin via Singlet Oxygen Generation. *Photochem. Photobiol.* **2009**, *85*, 1391−1399.
(63) Hussain, A.; Gadadhar, S.; Goswami, T. K.; Karande, A. A.; Chakravarty, A. R. Photoactivated DNA Cleavage and Anticancer

Activity of Pyrenyl-Terpyridine Lanthanide Complexes. *Eur. J. Med. Chem.* **2012**, *50*, 319−331.
(64) Silva, R.; Carmo, H.; Dinis-Oliveira, R.; Cordeiro-da-Silva, A.; Lima, S. C.; Carvalho, F.; Bastos Mde, L.; Remiao, F. In Vitro Study of P-Glycoprotein Induction as an Antidotal Pathway to Prevent Cytotoxicity in Caco-2 Cells. *Arch. Toxicol.* **2011**, *85*, 315−326.
(65) Frens, G. Controlled Nucleation for the Regulation of the Particle Size in Monodisperse Gold Suspensions. *Nature* **1973**, *241*, 20−22.
(66) Hurst, S. J.; Lytton-Jean, A. K. R.; Mirkin, C. A. Maximizing DNA Loading on a Range of Gold Nanoparticle Sizes. *Anal. Chem.* **2006**, *78*, 8313−8318.